JOURNAL OF GEOPHYSICAL RESEARCH, VOL. 107, NO. B2, 2028, 10.1029/2001JB000301, 2002

Frictional-viscous flow of phyllosilicate-bearing fault rock: Microphysical model and implications for crustal strength profiles

Bart Bos[1] and Christopher J. Spiers

High Pressure and Temperature Laboratory, Faculty of Earth Sciences, Utrecht University, Utrecht, Netherlands

Received 8 August 2000; revised 20 August 2001; accepted 20 August 2001; published 1 February 2002.

[1] It is widely believed that around the brittle-ductile transition, crustal faults can be significantly weaker than predicted by conventional two-mechanism brittle-ductile strength envelopes. Factors contributing to this weakness include the polyphase nature of natural rocks, foliation development, and the action of fluid-assisted processes such as pressure solution. Recently, ring shear experiments using halite/kaolinite mixtures as an analogue for phyllosilicaterich rocks for the first time showed frictional-viscous behavior (i.e., both normal stress and strain rate sensitive behavior) involving the combined effects of pressure solution and phyllosilicates. This behavior was accompanied by the development of a mylonitic microstructure. A quantitative assessment of the implications of this for the strength of natural faults has hitherto been hampered by the absence of a microphysical model. In this paper, a microphysical model for shear deformation of foliated, phyllosilicate-bearing fault rock by pressure solution-accommodated sliding along phyllosilicate foliae is developed. The model predicts purely frictional behavior at low and high shear strain rates and frictional-viscous behavior at intermediate shear strain rates. The mechanical data on wet halite + kaolinite gouge compare favorably with the model. When applied to crustal materials, the model predicts major weakening with respect to conventional brittle-ductile strength envelopes, in particular, around the brittle-ductile transition. The predicted strength profiles suggest that in numerical models of crustal deformation the strength of high-strain regions could be approximated by an apparent friction coefficient of 0.25–0.35 down to depths of 15–20 km. *INDEX TERMS:* 5104 Physical Properties of Rocks: Fracture and flow; 8005 Structural Geology: Folds and folding; 8045 Structural Geology: Role of fluids; 8159 Evolution of the Earth: Rheology—crust and lithosphere

1. Introduction

[2] Field observations show that crustal deformation is mostly localized into narrow fault or shear zones. In numerical modeling of crystal dynamics, crustal rheology is generally represented using a two-mechanism strength profile. The upper parts of the crust are modeled using a brittle-frictional faulting rheology, whereas the lower parts are described using power law creep equations describing crystal plastic flow of quartz or feldspar [*Goetze and Evans*, 1979; *Govers and Wortel*, 1995; *Kohlstedt et al.*, 1995; *Ranalli*, 1997]. This approach leads to a crustal or fault zone strength profile of the type shown schematically in Figure 1.

[3] Though widely used, it has long been realized that this two-mechanism description of crustal rheology is drastically oversimplified, notably regarding the transition between brittle/frictional and ductile behavior (loosely termed the brittle-ductile transition here). First, such strength profiles are based on flow laws for monomineralic materials obtained from relatively low strain experiments. However, natural fault/shear zones are polymineralic, with individual minerals going through a brittle-ductile transition at different depths [*Handy*, 1990; *Handy et al.*, 1999] and with mineral reactions progressively producing significant portions of weak phyllosilicates [e.g., *Wintsch et al.*, 1995]. In addition, with increasing strain, fault rocks often become foliated, allowing alignment and interconnection of weaker phases, in particular the phyllosilicates, with associated effects on bulk rheology [*Shea and Kronenberg*, 1992, 1993]. Furthermore, under the hydrothermal conditions pertaining around the brittle-ductile transition, where frictional sliding is inhibited by high confining pressures and crystal plastic flow by low-to-moderate temperatures, fluid-assisted deformation processes such as pressure solution are operative [*Rutter*, 1983; *Schwarz and Stöckhert*, 1996; *Stewart et al.*, 2000] and may significantly reduce long-term fault strength [*Sibson*, 1977, 1983; *Lehner and Bataille*, 1985; *Chester and Higgs*, 1992; *Hickman et al.*, 1995]. Taken together, the above phenomena are expected to lead to truncation of the strength maximum at the brittle-ductile transition predicted by "classical" two-mechanism strength profiles, as qualitatively indicated in Figure 1 [*Sibson*, 1983; *Chester*, 1995; *Hickman et al.*, 1995]. Such a truncation of the strength profile can be expected to have a strong influence on the results of numerical modeling work on crustal dynamics, since the brittle-ductile transition region is the main load-bearing region of the crust. Moreover, a realistic description of the mechanical behavior of fault zones at depths down to the brittle-ductile transition is imperative for understanding the seismic cycle. Despite the importance of the anticipated weakening effects in the brittle-ductile transitional region, however, very little quantitative information is available on these effects particularly regarding the effects of fluid-assisted deformation processes.

[4] In previous studies *Bos et al.* [2000] and *Bos and Spiers* [2001] reported frictional-viscous flow behavior of phyllosilicate-bearing simulated fault gouge (halite + kaolinite) sheared under conditions where pressure solution and cataclasis dominate over dislocation creep. By frictional-viscous behavior we mean shear deformation behavior in which the shear stress shows a significant

---

[1] Now at TNO TPD Materials Technology, Eindhoven, Netherlands.

0148-0227/02/2001JB000301$09.00

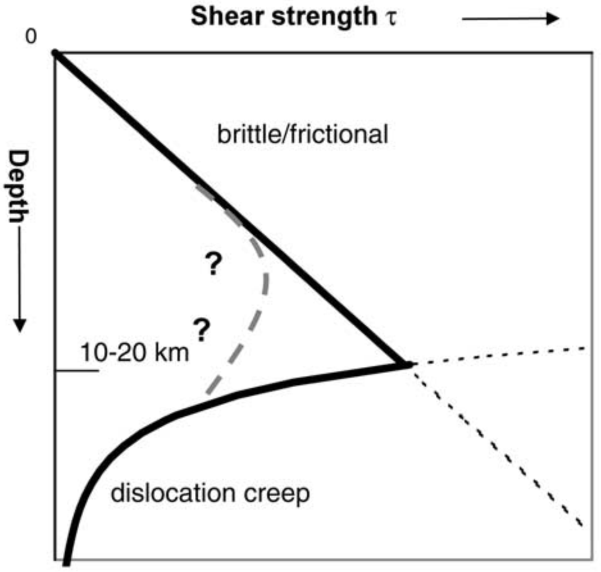

Figure 1. Schematic diagram showing the crustal strength profile defined by relations describing brittle/frictional behavior (Byerlee's law) and dislocation creep (solid lines). The hypothesized weakening around the brittle-ductile transition is shown by the dashed shaded line. The profile is drawn for a single uniform strain rate and can be viewed as applying to bulk crust or to fault zones.

dependence on both normal stress and strain rate. In our experiments, a transition was observed from purely frictional behavior at low strain to frictional-viscous behavior at high strain. This transition was accompanied by the development of an anastomosing, foliated microstructure, strongly reminiscent of natural S-C mylonites [*White et al.*, 1980; *Lister and Snoke*, 1984]. It was inferred that the observed rate-dependent behavior occurred by a mechanism involving frictional sliding of the elongate halite clasts on the intervening kaolinite-rich foliae, with geometrical incompatibilities accommodated by pressure solution. The experiments provided, for the first time, experimental evidence of steady state fault creep accommodated by pressure solution, a mechanism that has been hypothesized for more than 2 decades [*Sibson*, 1977; *Rutter and Mainprice*, 1979; *Lehner and Bataille*, 1984/1985]. The experiments also provided evidence that such a mechanism is strongly enhanced by or maybe even critically dependent upon the presence of phyllosilicates. This is supported by recent field studies, which suggest that solution transfer processes play an important role in allowing low stress, ductile deformation of phyllonite strands in major shear zones [*Schwarz and Stöckhert*, 1996; *Imber et al.*, 1997; *Stöckhert et al.*, 1999; *Stewart et al.*, 2000] under conditions where nonfoliated or phyllosilicate-poor fault rocks show no significant ductile deformation. Several other studies have reported frictional-viscous behavior with increasing temperature or decreasing strain rate in halite/calcite mixtures [*Shimamoto*, 1989; *Kawamoto and Shimamoto*, 1998] and in serpentinite gouge [*Reinen et al.*, 1994]. Our observations differ from these in the sense that in our case, frictional-viscous behavior was due to pressure solution, whereas the viscous component in the studies of the *Shimamoto* [1989], *Kawamoto and Shimamoto* [1998], and *Reinen et al.* [1994] was inferred to be due to crystal plasticity of the weakest phase.

[5] To assess quantitatively the importance of the frictional-viscous sliding behavior reported by *Bos et al.* [2000] and *Bos and Spiers* [2001] for the long-term strength of natural phyllosilicate-bearing fault zones and to assess the implications of pressure solution-controlled fault creep for crustal strength profiles, a microphysically based model describing such behavior is needed. The aim of this paper is to develop such a model for fault rock deformation by frictional sliding along phyllosilicate foliae, with accommodation of microscale geometrical incompatibilities by pressure solution. The model predictions are subsequently compared with our data on the behavior of halite-kaolinite gouge. Finally, the model is applied to quartz-mica rocks in order to estimate the effect of pressure solution-controlled frictional-viscous behavior on the strength of faults in the continental crust.

2. Previous Data on Frictional-Viscous Flow Behavior

[6] In our previous experiments on simulated fault gouge [*Bos and Spiers*, 1999; *Bos et al.*, 2000; *Bos and Spiers*, 2001], brine-

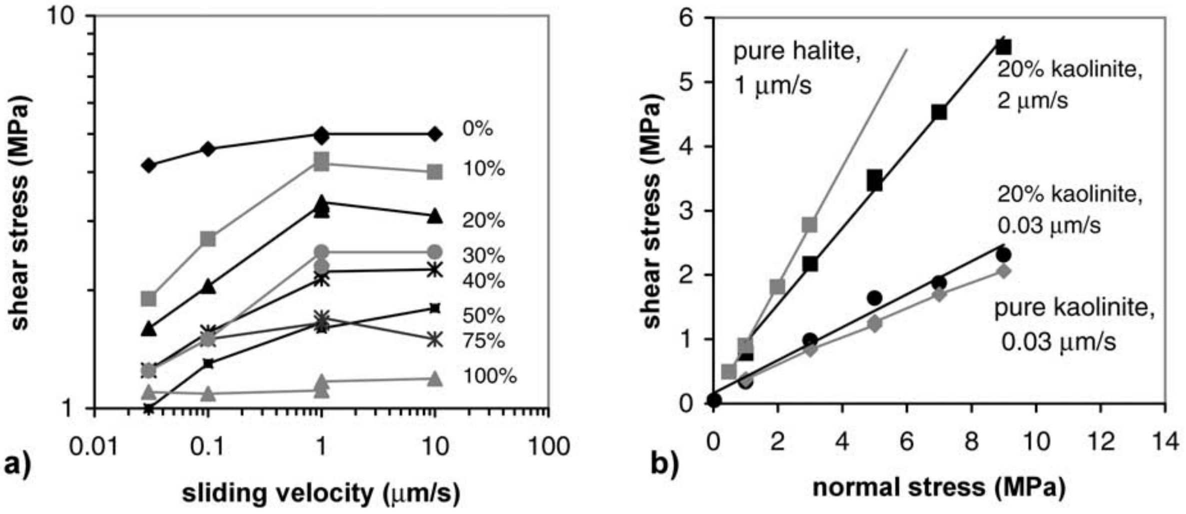

Figure 2. Data obtained from experiments on brine-saturated halite/kaolinite mixtures (reprinted from *Bos et al.* [2000] with permission from Excerpta Medica Inc.). For comparison, data on brine-saturated pure halite and pure kaolinite gouge are shown as well. (a) Shear stress versus sliding velocity. Normal stress is 5 MPa, kaolinite content is as indicated. (b) Shear stress versus normal stress. Kaolinite content and sliding velocity are as indicated. Note that frictional-viscous flow behavior is observed in halite + kaolinite mixtures at velocities below 1 μm s^{-1} and that the apparent friction coefficient is dependent on sliding velocity (the slope of the line through the data in Figure 2b).

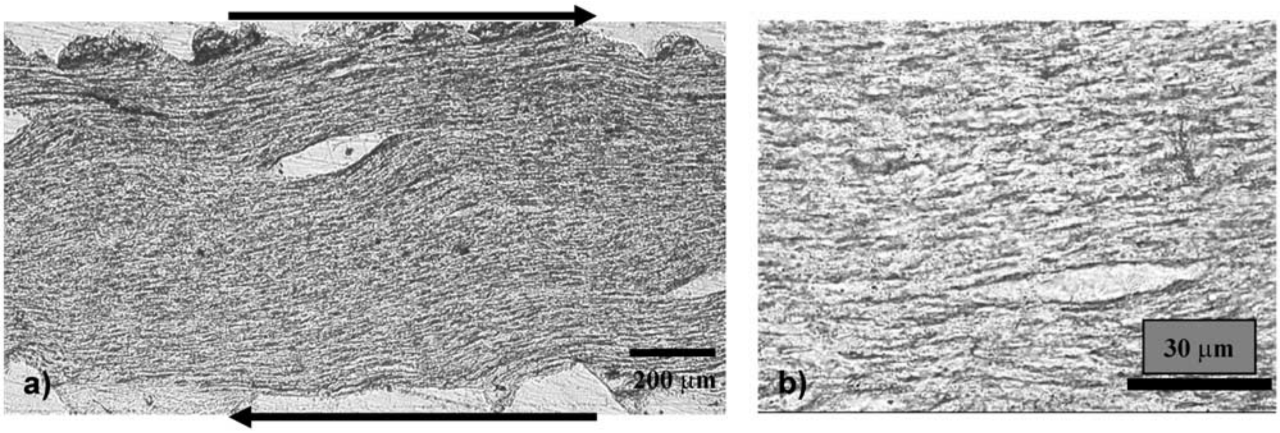

Figure 3. (a) Typical microstructure of material deformed in the rate-sensitive regime at sliding velocity 0.2 μm s^{-1} and 5 MPa normal stress. Shear sense is dextral; the shear plane is horizontal. The microstructure shows elongated clasts embedded in fine-grained, foliated matrix. Total shear strain in this sample is 100. The orientation of the long axis of the strain ellipse is at 0.6° to the shear direction, i.e., virtually horizontal. (b) Detailed microstructure of matrix. (Reprinted from *Bos and Spiers* [2001] with permission from Excerpta Medica Inc.)

saturated porous mixtures of halite and kaolinite were sheared to high strains (shear strains up to 1000) in a rotary shear apparatus at room temperature, under conditions favoring pressure solution in wet halite, with negligible dislocation creep. The experiments were performed at constant shear displacement, constant normal stress, and constant pore fluid pressure (1 atm) and were performed using displacement rate and normal stress stepping methods. The data showed a transition from frictional behavior at small displacements to quasi steady state frictional-viscous behavior at large displacements (>20 mm, shear strain ~35), the transition being accompanied by significant strain weakening. The mechanical behavior observed at high strains, where steady state strength was reached, is illustrated in Figures 2a and 2b. These data show that halite-kaolinite gouge exhibited strongly rate-dependent steady state sliding behavior at low (<1 μm s^{-1}) sliding velocities. In contrast, purely frictional behavior (shear strength linearly dependent on normal stress and insensitive to sliding rate) was observed in pure kaolinite and pure halite gouge, showing that the rate-dependent behavior requires the presence of both halite and kaolinite. Moreover, it was observed that halite-kaolinite gouges saturated with an inert pore fluid also behave in a purely frictional manner, demonstrating that the rate-sensitive behavior must be due to a fluid-assisted deformation mechanism.

[7] The microstructure of halite-kaolinite mixtures at mechanical steady state is shown in Figure 3a. Shear sense is dextral, and the shear plane is horizontal. Typically, the deformed gouge consists of isolated, augen-like clasts embedded in a contiguous, fine-grained halite-kaolinite matrix. The matrix consists of elongate, ribbon-shaped halite grains, surrounded by an anastomosing network of kaolinite. The material shows a wavy foliation, with regions displaying an oblique foliation alternating laterally with shear band-like zones, with subhorizontally to synthetically oriented foliation. On average, the foliation is nearly horizontal. Experiments performed to study the microstructural evolution of these gouges with shear strain [*Bos and Spiers*, 2001] showed that the establishment of the contiguous network of halite-kaolinite matrix material coincides with the onset of mechanical steady state. This suggests that steady state strength is controlled mostly by the rheology of the fine-grained matrix. Moreover, the microstructure of the fine-grained matrix was observed to remain essentially constant up to shear strains exceeding 1000 [*Bos and Spiers*, 2001]. Figure 3b shows a detail of the matrix. Note that neither grain shape nor foliation orientation track the finite strain ellipse, since in that case the foliation would be horizontal everywhere and the grains much more elongate. This implies that shear deformation within the matrix was inhomogeneous. It was proposed that deformation occurred by a mechanism involving sliding of halite grains along anastomosing, phyllosilicate-rich foliae, with accommodation by pressure solution of the halite clasts and matrix grains [*Bos et al.*, 2000]. Deformation in the regions with oblique foliation and deformation within the shear bands were probably coupled such that volume changes were minimal. A component of subcritical crack growth may also have contributed to the observed rate-dependent behavior, but the lack of significant grain size reduction in the matrix with progressive strain [*Bos and Spiers*, 2001] implies that cataclasis due to this process is of little importance.

[8] In section 3 a microphysical model describing shear deformation by pressure solution-accommodated sliding is developed. For this purpose, we assume that the average foliation orientation is horizontal. In the case of halite the constitutive kinetic parameters for pressure solution are well constrained [*Spiers et al.*, 1990]. Hence our model can be tested by comparing its predictions with the mechanical behavior observed in our previous experiments on halite/kaolinite gouge.

3. Model Development

3.1. Model Geometry and Kinematics

[9] Figure 4a shows a schematic diagram of our model steady state matrix microstructure for a volume of bulk fault rock undergoing simple shearing at a rate $\dot{\gamma}$ under the action of a shear stress τ and at effective normal stress σ_n. A contiguous, anastomosing network of phyllosilicate foliae surrounds elongate grains of a soluble solid. The phyllosilicates define wavy foliation planes that are horizontal on average. Figure 4b shows one wavelength of phyllosilicate-covered foliation plane (bold line). The amplitude of the foliation "waves" is denoted as h, the wavelength is $2d$, and the leading edge of the grains is inclined at an angle α to the shear plane. Pore fluid is assumed to be present in a connected pore network at a uniform pressure P_f. The system is assumed to be chemically closed.

[10] While the matrix grains and foliae are drawn with uniform geometry in Figure 4a, we assume that local microstructural fluctuations imply that at any moment in time, shear deformation of the material occurs by sliding along throughgoing phyllosilicate foliation surfaces (average spacing s), with negligible deformation of the "microlithons" in between, within which sliding is locked

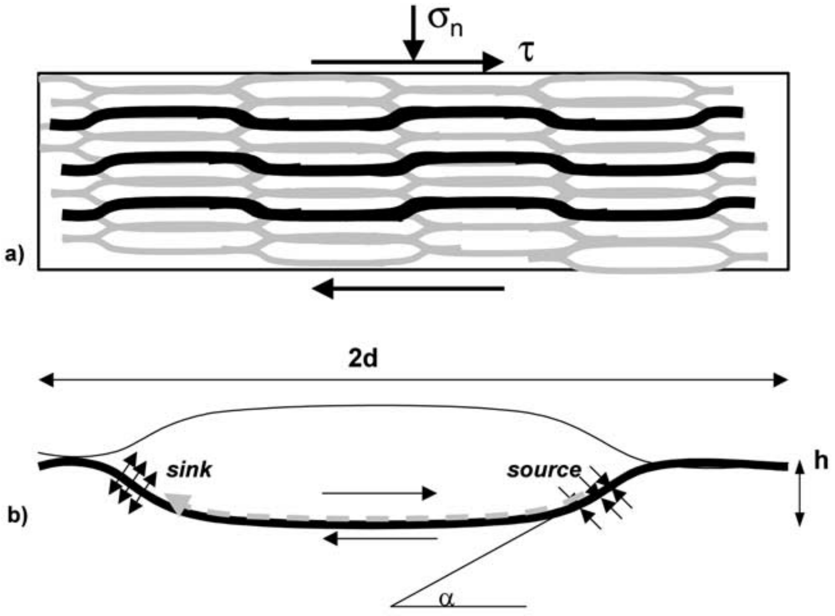

Figure 4. (a) Schematic diagram of model microstructure, showing contiguous, anastomosing network of phyllosilicates separating elongate halite grains. The structure is transected by widely spaced actively sliding phyllosilicate foliation planes (indicated by solid lines), which are horizontal, on average. (b) Schematic drawing of sliding surface element, the active sliding surface shown by the bold line. Shear sense is dextral. The diffusive mass flux from source (leading edge) to sink (trailing edge) regions is indicated by the dashed arrow. The foliation waves have amplitude h; the grains have long axis d. The leading edge of the grain is inclined at angle α to the horizontal.

because of microstructural irregularity. For simplicity, it is assumed that active foliation planes are not connected. Shear movement along the active foliation planes involves frictional sliding along the horizontal parts of the wavy foliation waves, accommodated by pressure solution, i.e., by diffusive mass transfer through fluid films and/or channels from the leading edges to the trailing edges of the foliation waves, in response to gradients in local contact normal stress (see Figure 4b). This is similar to the case of diffusion-accommodated grain boundary sliding along a sinusoidal surface as modeled by *Raj and Ashby* [1971] but includes frictional sliding along the horizontal parts of the foliation surfaces as an additional dissipative process. As indicated already, we assume a bulk simple shear deformation geometry. Thus there are no bulk volume/mass changes (chemically closed system) and no lateral displacements. All microscale mass transfer paths accordingly lie in the plane of Figure 4a. The two-dimensional (2-D) nature of our assumed microstructure clearly departs from reality in that the matrix grains are effectively "infinite" in extent normal to Figure 4a. However, since successive 2-D sections of a fault rock microstructure would be essentially equivalent in morphology, we consider our assumed microstructure to be a reasonable approximation of a spatially and time-statistically average situation. The limitation is that detailed three-dimensional microstructural evolution (such as lineation development) is neglected.

[11] In the framework of the assumed microstructure and kinematics, sliding along the horizontal parts of the active foliation planes and accommodation of sliding by pressure solution are clearly coupled processes: Matter must be dissolved at the leading edge of grains for sliding to occur on the horizontal segments of the active phyllosilicate foliae. This situation can be represented in terms of the mechanical analogue system drawn in Figure 5a. Here a frictional slider (marked A, representing the contribution of frictional sliding along phyllosilicate foliae to total shear stress) and a dashpot (marked B, representing the time-dependent pressure solution process) are connected in parallel such that the strongest makes the largest contribution to the overall strength. This rheological model predicts rate-independent behavior at low shear strain rates, where accommodation of sliding by pressure solution is relatively easy. At higher shear strain rates, pressure solution will take over as the strength-determining mechanism, leading to increasing total shear strength with increasing shear strain rate.

[12] At still higher strain rates, however, a shear stress level will be reached at which material dilatation is easier than continued deformation because of pressure solution-controlled sliding on foliation surfaces. At this stress level a transition will occur to deformation by a mechanism involving dilatation, cataclasis, and faulting of gouge. The shear stress level at which transition will occur is the limiting shear stress for the onset of dilatation. This is supported by our previous experimental data. These show that upon stepping shear strain rate into the rate-insensitive regime, significant transient dilatation occurs, whereas no significant volume changes are associated with the rate-sensitive regime [*Bos et al.*, 2000].

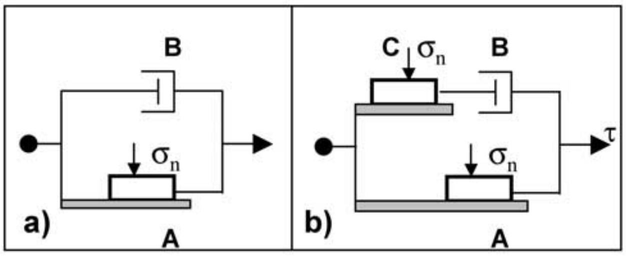

Figure 5. (a) Mechanical analogue diagram for the deformation process at zero porosity. Element A represents frictional sliding along phyllosilicate foliae; element B represents pressure solution. (b) Mechanical analogue diagram including effect behavior at critical stress for the onset of dilatation (element C), see text for discussion.

[13] The limiting shear stress at which dilatation starts contains a contribution due to frictional sliding along foliation surfaces and a contribution due to work against normal stress and, strictly speaking, also a (small) contribution due to the creation of new surface area. Instead of modeling the processes at the limiting stress level in detail, the behavior occurring around the critical shear stress at which dilatation starts may be incorporated in the mechanical analogue description by inserting an additional frictional slider C, as shown in Figure 5b. This slider does not physically represent a frictional sliding process in the gouge but rather represents the work against normal stress that would be required for dilatation. The contribution of new surface area creation is neglected. Element C acts in series with the dashpot representing pressure solution leading to shear (element B), thus limiting the stress on the dashpot to be at or below the dilatation criterion. In this way, we dictate a limiting stress level in our model above which the process of pressure solution-accommodated sliding is replaced by other processes without modeling the processes that occur at higher sliding velocities. However, these processes are (to a first order) insensitive to strain rate and temperature, so we believe that the behavior at least around the shear strain rate corresponding to the limiting stress for dilatation can be reasonably well approximated by a frictional slider.

[14] By including a limiting stress in this way, it is implicitly assumed that slider A represents the contribution of grain boundary frictional sliding to total shear resistance both at and below the dilatation stress criterion. This is not necessarily correct in detail. However, for simplicity, we will assume that in both cases the actively sliding areas are roughly the same size.

[15] Now at low sliding velocities in the situation depicted in Figure 5b, grain contact sliding (element A) is accompanied by pressure solution (element B), and element C is inactive. Clearly, the total stress will be dominated by element A at the lowest velocities, leading to frictional behavior, and by element B at higher velocities, leading to viscous behavior. At even higher velocities the shear stress becomes high enough for the strength of C (the dilatation criterion) to be exceeded. At this point the stress in the upper branch of Figure 5b is constrained to remain at the level dictated by element C, i.e., to remain at the threshold of dilatation. In section 3.2, we will develop a rheological model based on Figure 5b.

3.2. Model Formulation

[16] From Figure 5b, during fault shear at constant strain rate, it follows from mechanical analogue theory [e.g., *Ranalli*, 1995] that the shear stress contributions of the different processes to the total shear stress τ are related via the equation

$$\tau = \tau_A + \left(\frac{1}{\tau_B} + \frac{1}{\tau_C}\right)^{-1}, \qquad (1)$$

where τ_A represents the shear stress contribution due to frictional sliding along the horizontal parts of the active phyllosilicate foliae, τ_B is the shear stress contribution due to pressure solution, and τ_C represents the work against normal stress needed to induce dilatation, as explained in section 3.1. In the following, we will derive expressions for the three contributions τ_A, τ_B, and τ_C.

[17] First, the shear stress contribution due to frictional sliding along the horizontal parts of the active phyllosilicate foliae, τ_A, can be written

$$\tau_A = P\mu_{gb}\sigma_n{}', \qquad (2)$$

where P is a factor expressing the proportion of the grain boundary area undergoing sliding (which is of order 3/4 in our model microstructure), μ_{gb} is an apparent grain boundary friction coefficient, and $\sigma_n{}'$ is the macroscopic effective normal stress. Since we assume throughgoing sliding surfaces, and the sliding parts of the active surfaces are assumed to be horizontal and of constant area, the macroscopic normal stress and the local normal stress on the horizontal sliding sections will be roughly the same, particularly when the strength contribution of element B is relatively small. The factor P thus represents a simple linear scaling factor linking the macroscopic shear strength contribution τ_A to the microscopic frictional strength of the horizontal portions of the phyllosilicate foliation. Note that, in general, the apparent grain boundary friction coefficient may represent sliding along phyllosilicate layers or sliding within the phyllosilicate layers. Grain boundary cohesion is assumed to be negligibly small, since phyllosilicates are thought to inhibit contact adhesion [*Bos and Spiers*, 2000; *Hickman and Evans*, 1995]. Instead of frictional intergranular sliding, a creep relation for basal dislocation glide within the phyllosilicates could also be inserted here if desired [*Kronenberg et al.*, 1990; *Mares and Kronenberg*, 1993].

[18] From our preceding considerations, τ_C equals the contribution to shear stress due to work that must be done against the effective normal stress to cause sample dilatation. In the framework we have defined, this can be approximated as

$$\tau_C = \sigma_n \tan\alpha, \qquad (3)$$

where α is defined in Figure 4b. Note that α is not the friction angle used in soil mechanics [e.g., *Wood*, 1990], which is a macroscopic parameter including grain boundary friction as well as the grain packing. In our case, α is a microstructural parameter accounting for dilatative work against normal stress, and the contribution to the limiting stress for dilatation by frictional sliding along the sliding surface is represented by element A in Figure 5b.

[19] To analyze the role of pressure solution (element B in Figure 5), we consider the volume represented in Figure 4b. The process of pressure solution involves the series-sequential steps of dissolution at source sites, diffusion through the grain boundary zone (phyllosilicate-halite interface), and precipitation at the sink sites. The grain boundaries are assumed to contain a fluid phase, either in the form of an adsorbed thin film [*Renard and Ortoleva*, 1997; *Rutter*, 1976] or in the form of a dynamically stable island-channel structure at the boundary between phyllosilicates and matrix grains [*Raj and Chyung*, 1981; *Raj*, 1982; *Lehner*, 1990; *Spiers and Schutjens*, 1990]. The grain boundary zone is characterized by an effective fluid thickness δ and an effective diffusion coefficient D. To derive a relation between the shear stress contribution due to pressure solution and the shear strain rate, we follow *Lehner and Bataille* [1984/1985] and *Spiers and Schutjens* [1990] in treating pressure solution as a nonequilibrium, dissipative process.

[20] Assuming no increase in internal energy or entropy during deformation, the first law of thermodynamics requires that the rate of external work done on the fault zone per unit volume equals the volume specific rate of dissipation ($\dot{\Delta}$) due to pressure solution [*De Groot and Mazur*, 1962; *Prigogine*, 1967; *Lehner and Bataille*, 1984/1985]. For isovolumetric, steady state conditions this can be written

$$\tau\dot{\gamma} = \dot{\Delta}, \qquad (4)$$

where τ is shear stress and $\dot{\gamma}$ is shear strain rate. Now the rate of energy dissipation due to pressure solution can be written as the product of mean mass flux and thermodynamic driving force [*Lehner and Bataille*, 1984/1985; *Spiers and Schutjens*, 1990], that is, as

$$\dot{\Delta} = \dot{M}\Delta\Pi. \qquad (5)$$

Here the flux $\dot{M}$ is the average source-to-sink mass transfer rate per unit volume of fault zone (kg m^{-3} s^{-1}), and the force is the average chemical potential difference between source and sink sites (J kg^{-1}) driving pressure solution (cf. Figure 4b). The expression for the dissipation due to steady state pressure solution is dependent on which of the processes of dissolution at source sites, diffusion through grain boundaries, and precipitation at sink sites is slowest and hence rate controlling. For the case of pressure solution in halite, diffusion is known to be the rate-controlling mechanism [*Spiers et al.*, 1990; *Spiers and Brzesowsky*, 1993]. To extend the applicability of our model to other materials, we derive expressions for the dissipation rate for both the diffusion-controlled and the interface reaction-controlled cases.

3.2.1. Pressure solution: Diffusion-controlled case.

[21] Grain boundary diffusion along the phyllosilicate foliae is governed by Fick's law, which can be written:

$$J = \rho_f D \mathrm{gradC} \tag{6}$$

where J is the mass flux (kg ms^{-1}), ρ_f is fluid density, and *gradC* is the (stress-induced) concentration gradient along the contact (concentration in units of mass fraction). At each actively dissolving grain leading edge, for a length w of grains normal to Figure 4a this flux acts through a diffusion window $w\delta$, where δ is the thickness of the assumed contact fluid layer. The rate of mass transfer per active leading edge (kg s^{-1}) is then

$$J^* = w\rho_f D\delta \mathrm{grad}C. \tag{7}$$

Using

$$\mathrm{grad}C = \frac{C_s M_s}{RT}\mathrm{grad}\Pi, \tag{8}$$

where C_s and M_s are the solubility and molar mass, respectively, of the solid, R is the gas constant and T is absolute temperature, and assuming the potential difference acts over an average diffusion distance d, the total mass flux per active leading edge (kg s^{-1}) becomes

$$\dot{m} = \frac{\rho_f w D\delta C_s M_s}{RTd}\Delta\Pi. \tag{9}$$

Now the number of foliation leading edges actively undergoing pressure solution in unit volume of fault zone is $N = A/(hwd)$, where A is a constant reflecting the proportion of foliation surfaces actively sliding at any instant of time. The total rate of mass transfer per unit volume of fault zone (kg m^{-3} s^{-1}) is then given by upscaling the microscopic mass transfer rate $\dot{m}$ by the factor N, yielding the macroscopic transfer rate

$$\dot{M} = N\dot{m} = \frac{A\rho_f D\delta C_s M_s}{RThd^2}\Delta\Pi. \tag{10}$$

Equation (10) constitutes the necessary volume specific relation between force and flux for the case of diffusion controlled pressure solution creep. Substituting for $\Delta\Pi$ from (5) then yields

$$\dot{\mathrm{D}}_d = \frac{RThd^2}{A\rho_f D\delta C_s M_s}\dot{M}^2. \tag{11}$$

[22] We now proceed to derive an equation relating the rate of mass transfer per unit volume of fault zone to the imposed shear strain rate. The shear strain rate can be written as

$$\dot{\gamma} = \frac{Av_{\mathrm{diss}}}{h}, \tag{12}$$

where v_{diss} is the average dissolution velocity of the leading edges in the direction of fault slip and A is the proportion of actively sliding foliation surfaces. Note that A/h is the average spacing of the phyllsilicate foliae. The mass transfer rate per leading edge is related to v_{diss} by

$$\dot{m} = hw\rho_s v_{\mathrm{diss}} \tag{13}$$

where ρ_s is the solid density and it is assumed that the area of dissolving contact is $hw/\sin\alpha$. Using the scaling relation $\dot{M} = N\dot{m}$ and substituting for v_{diss} from (12) into (13), the mass transfer rate per unit volume of gouge can be expressed as a function of strain rate by

$$\dot{M} = \frac{h\rho_s}{d}\dot{\gamma}. \tag{14}$$

Equation (14) can now be substituted into (11) to yield the final expression for the rate of dissipation due to diffusion-controlled pressure solution. Also making use of

$$\frac{\rho_s}{M_s} = \frac{1}{\Omega_s}, \tag{15}$$

where $_s$ is the molar volume of the solid, we obtain

$$\dot{\Delta}_d = \frac{\alpha\rho_s RTh^3}{\rho_f D\delta C_s\Omega_s}\dot{\gamma}^2. \tag{16}$$

Combining this with (4) and using $d = Bh$, where B is the aspect ratio (length/width) of the matrix grains, yields the following expression for the shear stress contribution due to diffusion-controlled pressure solution:

$$\tau_d = \frac{\rho_s RTd^3}{B^3\rho_f D\delta C_s\Omega_s}\dot{\gamma}. \tag{17}$$

3.2.2. Pressure solution: Interface reaction-controlled case.

[23] For the kinetics of dissolution or precipitation a phenomenological relationship of the form

$$v_{s,p} = k_{s,p}M_s\left(\frac{\Delta\Pi}{RT}\right)^n \tag{18}$$

is postulated [*Lehner and Bataille*, 1984/1985] in accordance with both theory and experimental data on dissolution/growth kinetics. Here k is a phenomenological rate coefficient, which may differ for dissolution (subscript s) and precipitation (subscript p). Following *Lehner and Bataille* [1984/1985], the exponent n is taken to be unity here, although this need not always be the case [cf. *De Meer and Spiers*, 1997]. Since the surface areas of dissolution and precipitation are roughly equal in our model geometry, the two processes must proceed at equal rates under closed system conditions. Therefore the analysis for the dissolution- and precipitation-controlled cases are essentially equivalent. As in the foregoing case of diffusion control, the microscopic mass transfer rate is written as a function of driving force using (13) and (18). This yields

$$\dot{m} = \frac{k_{s,p} M_s h w \rho_s}{RT} \Delta\Pi. \tag{19}$$

Again, using $\dot{M} = N\dot{m}$ and substituting for from (5), the volume-specific rate of dissipation due to dissolution or precipitation reactions can be written in terms of the mass transfer rate per unit volume of fault zone $\dot{M}$ as

$$\dot{\Delta}_{s,p} = \frac{RTd}{A k_{s,p} \rho_s M_s} \dot{M}^2. \tag{20}$$

Again using (14), (15), and (4), the relation between shear stress and strain rate for interface reaction-controlled pressure solution can be written

$$\tau_{s,p} = \frac{RTd}{B^2 k_{s,p} \Omega_s} \dot{\gamma}. \tag{21}$$

3.2.3. Final model. [24] We now use the above expressions for the shear stresses τ_A, τ_C, and $\tau_B = \tau_{d,s,p}$ to obtain the complete model for shear deformation of phyllosilicate-rich fault rock under conditions favoring pressure solution. To do this, we substitute (2), (3), and either (17) or (21) into (1). This yields

$$\tau = P\mu_{gb}\sigma_n + \frac{\sigma_n K_d \dot{\gamma} \tan\alpha}{\sigma_n \tan\alpha + K_d \dot{\gamma}} \tag{22}$$

for the case of diffusion-controlled pressure solution, where K_d is a kinetic factor, defined by

$$K_d = \frac{\rho_s RTd^3}{B^3 \rho_f D\delta C_s \Omega_s}. \tag{23}$$

For the case of interface reaction-controlled pressure solution the expression is

$$\tau = P\mu_{gb}\sigma_n + \frac{\sigma_n \tan\alpha K_{s,p} \dot{\gamma}}{\sigma_n \tan\alpha + K_{s,p} \dot{\gamma}}, \tag{24}$$

where $K_{s,p}$ is defined as

$$K_{s,p} = \frac{RTd}{B^2 k_{s,p} \Omega_s}. \tag{25}$$

4. Application to the System Halite Plus Kaolinite

[25] In this section, we illustrate the general behavior predicted by the model by applying it using parameter values appropriate for a halite + kaolinite gouge. We then compare the model predictions with our experimental data on halite + kaolinite gouge. For the value of the grain boundary friction coefficient (μ_{gb}) we use *Bos et al.*'s [2000] previously measured friction coefficient for wet kaolinite gouge, i.e., 0.2. This value is low compared with other experiments on wet kaolinite gouge, performed at higher pressures, in which values of 0.4–0.6 were measured [*Rutter*, 1979; *Rutter and Maddock*, 1992; *Morrow et al.*, 2000]. However, it should be noted that the friction coefficient measured in experiments on gouge layers is not necessarily equal to the grain/phyllosilicate or phyllosilicate-phyllosilicate interfacial friction coefficient, since the measured friction coefficient of gouge may be determined by gouge microstructure as well as by intrinsic grain boundary friction. The kaolinite-rich gouges that yielded friction values of 0.4–0.6 show distributed deformation and the formation of a steep foliation and R shears [*Rutter*, 1979; *Rutter et al.*, 1986]. Unfortunately, *Morrow et al.* [2000] did not show the microstructure of their deformed samples. In our pure kaolinite experiments, deformation was localized on a horizontal boundary Y shear. This could explain our lower friction coefficient, since sliding along the foliation in an obliquely foliated gouge requires dilatation in addition to overcoming grain boundary friction, both of which will contribute to the measured shear stress. This implies that our measured value of kaolinite friction is probably closer to the intrinsic grain boundary friction coefficient of wet kaolinite than obtained in studies showing distributed deformation. The experiments of *Morrow et al.* [2000] showed a significant lubrication effect of water in various phyllosilicate minerals. The weakening/lubrication effect on kaolinite due to the addition of water measured in our experiments [*Bos et al.*, 2000] is similar in magnitude to that reported by *Morrow et al.* [2000] (i.e., a reduction in μ of 0.2). Since it is the grain boundary friction coefficient and not the microstructure that is likely to be instantaneously influenced by the addition of fluid, this observation again suggests that the difference between our friction values and other findings can be attributed to microstructural factors.

[26] Pressure solution in halite is known to be diffusion controlled. The effective diffusion factor $D\delta$ was determined by *Spiers et al.* [1990] for halite-halite grain boundaries and by *Hickman and Evans* [1995] for halite-silica interphase boundaries. Both studies obtained a value of the order of 4×10^{-19} m^3 s^{-1}. Experimental data indicate that the presence of clays at halite grain contacts causes a fivefold increase in the rate of pressure solution [*Hickman and Evans*, 1995]. Assuming that this effect is due to enhanced grain boundary diffusion, we multiplied the diffusion factor mentioned above by a factor 5. We chose a value for d of 20 μm, representative of the average grain size in the matrix of our sheared samples (see Figure 3b), and we took the average aspect ratio B to be 5. Finally, the proportion of actively sliding foliation planes was assumed to be 0.5.

[27] The general behavior predicted by our model at room temperature is illustrated in Figure 6. Figure 6a shows shear stress versus sliding velocity for various dilatation angles α and grain sizes d. Three regimes of behavior can be identified, as already anticipated qualitatively. At high slip rates (regime 3 in Figure 6a), shear stress is insensitive to shear strain rate. This is the region where, in our model, shear strength is controlled by elements A and C (see Figure 5b), and the predicted strength is simply the sum of the sliding surface friction coefficient and tan α, multiplied by the normal stress. We will refer to this value as the maximum shear strength. With decreasing sliding velocity a regime is entered where the shear strength is strongly strain rate sensitive (regime 2). This is the region where shear stress is controlled by pressure solution (element B) and to some extent by grain boundary sliding friction (element A). Note that although a linear shear stress versus strain rate relation was inserted for the pressure solution process, the shear stress predicted by the model does not show linear viscous behavior (see Figure 6a) in any strain rate interval; instead, the maximum predicted value of the strain rate sensitivity m is ~0.3, rather than the value of 1 expected for linear viscous behavior. Finally, at low velocities (regime 1) the model predicts shear strength to be independent of sliding velocity, as found at high velocities, but the strength is much lower. In this region, pressure solution is relatively fast and shear stress is determined mainly by the

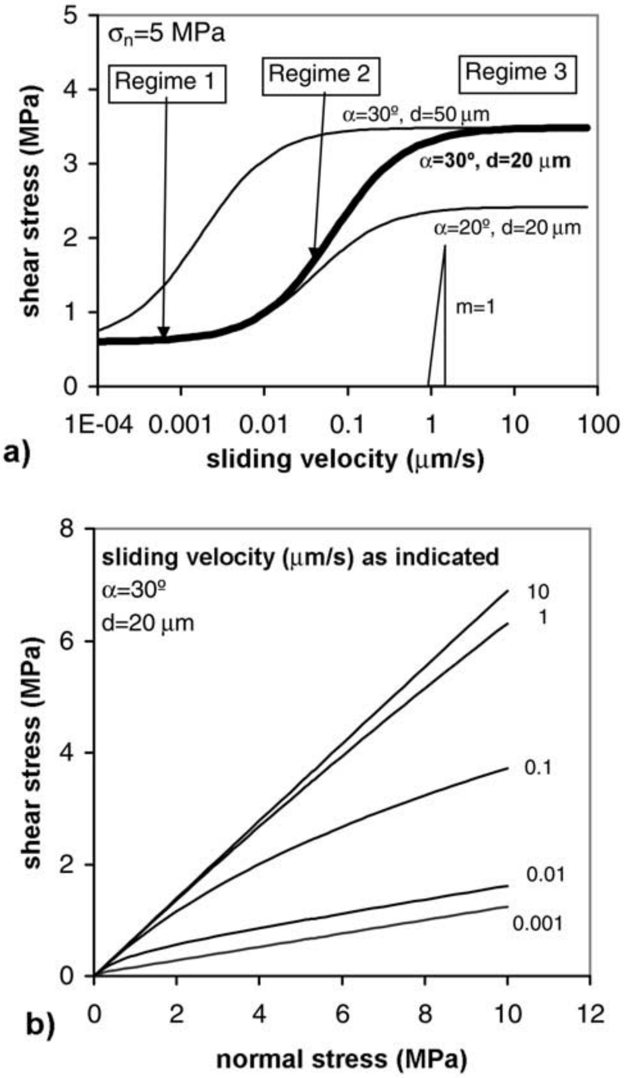

Figure 6. (a) Model predictions for halite/kaolinite gouge at 5 MPa normal stress. Values for ά and grain size *d* used are indicated. The hypotenuse of the triangle on the lower right side of the figure indicates the slope corresponding to a linear viscous rheology. Three regimes of behavior can be identified. With reference to Figure 5, at high velocities a frictional regime is predicted, with strength dominated by elements A and C. At intermediate velocities a strongly rate dependent regime is dominated by element B, and at low velocities a frictional regime is dominated by element A. (b) Predicted shear stress versus normal stress behavior. Note strong rate sensitivity of apparent friction coefficient (i.e., the slope of the lines), in particular at sliding velocities between 1 and 0.01 μm s^{-1}.

sliding surface friction coefficient. We will refer to this value as the "minimum shear strength."

[28] It can be seen from Figure 6a that the value of the maximum shear stress, as well as the maximum strain rate sensitivity reached, is strongly dependent on the chosen value of α. Increasing the grain size does not change the values of maximum and minimum shear stress but shifts the transition between them to lower strain rates. Figure 6b shows the predicted shear stress versus normal stress behavior. The apparent friction coefficient (i.e., the slope of the plot) is predicted to be strongly strain rate sensitive, in particular at velocities corresponding to regime 2 in Figure 6a.

[29] The model predictions are now compared with our data on halite + kaolinite gouge. A complication arises here since in the experiments, different clay contents were used, whereas clay content was not incorporated as a parameter in our model. However, from the gouge microstructures [cf. *Bos et al.*, 2000, Figure 11] it can be seen that the average foliation angle á decreases with increasing clay content. Figure 7 shows shear stress versus sliding velocity, with our data points for gouges containing 10, 30, and 50% kaolinite. The dashed lines are model predictions for values of α of 30°, 20°, and 10°, which we consider roughly representative of the microstructure of gouges with kaolinite contents of 10, 30, and 50%. It can be seen from Figure 7 that reasonable agreement is obtained between the model and our experimental data. The strength values predicted by the model fall in the range of the observed values. Moreover, the velocity range of rate-dependent behavior (regime 2) predicted by the model is similar to that observed in our data. The model fits the data particularly well for low-to-intermediate clay contents (10 and 30%), where the rate sensitivity of strength was strongest.

[30] Note from Figure 7 that at velocities above 1 μm s^{-1} the model tends to overestimate the strength measured in our experiments. This may be due to the fact that deformation at high velocities involves cataclasis and/or faulting, as discussed in section 3.1. In addition, the fit of the model to our data is not particularly good for high clay contents. A feature of the model that is not observed in the data is the low-velocity regime of rate-independent strength. This may be due to the fact that the imposed sliding velocities were not low enough. To verify this, experiments are needed on an apparatus with which even slower sliding rates can be attained. Alternatively, a smaller initial halite grain size could be used.

[31] Finally, we note that the fit of our model to the data, though seemingly reasonable, should be viewed with some caution. As demonstrated by Figure 7, the model is strongly sensitive to the chosen values for the angle α and grain size *d*, parameters which show considerable spread and are spatially inhomogeneous in our samples. Nevertheless, we believe that the rough agreement between the model and our data strongly supports our inference that deformation in our samples indeed occurred by a mixed grain boundary sliding plus pressure solution mechanism, at least at sliding velocities of 1 μm s^{-1} and lower and at clay contents <50%.

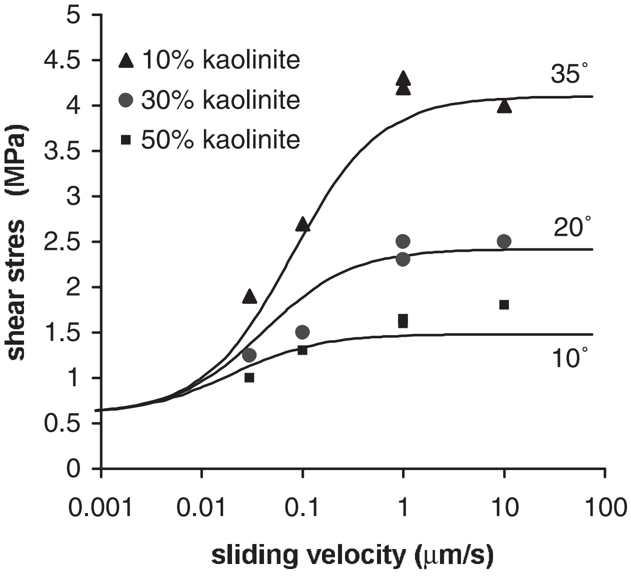

Figure 7. Comparison of model with data obtained from experiments on halite + kaolinite gouges. Model curves are shown for values of α of 10°, 20°, and 30°. Data are shown for kaolinite contents of 10, 20, and 30%.

5. Application to Natural Faults: A Strength Profile for Zones of High Strain

[32] In this section, our model is applied to natural fault rock in order to provide a quantitative indication of the effect of the pressure solution-controlled creep process on the strength of crustal fault rock. The model is applied to four different tectonic settings: (1) a transcrustal strike slip fault zone (such as the San Andreas fault zone), (2) a normal fault zone accommodating crustal extension, (3) a thrust fault zone deforming under high pressure, low-temperature conditions typical of a subduction setting, and (4) a thrust fault zone deforming under intermediate conditions typical of continent-continent collision zones. The strength profiles shown are not meant to be applied directly to a particular region or fault zone but rather are meant to illustrate the relative importance of pressure solution-controlled fault slip in different thermal settings.

5.1. Model Parameters

[33] The geothermal gradients chosen for the models are 25°C km^{-1} for case 1, consistent with heat flow data from the San Andreas Fault Zone region [*Lachenbruch and Sass*, 1980; *Sibson*, 1983], 35° km^{-1} for case 2, 15°C km^{-1} for case 3 [*Schwarz and Stöckhert*, 1996], and 25°C km^{-1} for case 4 [*Spear*, 1993]. For these examples, we assume hydrostatic pore pressure at all depths, as is usually done in studies of crustal rheology. It should be noted that field evidence indicates that, at least locally, fluid pressures may be considerably higher than this. In such case, our model thus provides an upper bound to fault rock strength. Crustal density is taken to be 2.75 g cm^{-3}. At upper crustal levels we will assume purely frictional behavior. For this region we used a coefficient of friction of 0.75, typical for a wide range of materials [*Byerlee*, 1978].

[34] The frictional strength of a fault is a function of the type of fault, the effective pressure, and the coefficient of friction. For the case of a strike-slip fault, we assume that the effective overburden pressure, σ_v, is the intermediate principal effective stress and is equal to the mean effective stress, i.e., $\sigma_v' = \frac{1}{2}(\sigma_1' + \sigma_3')$, where σ_1' and σ_3' are the maximum and minimum principal effective stresses, respectively. In this case, the minimum differential stress $(\sigma_1' - \sigma_3')$ to activate sliding is [*Sibson*, 1974; *Ranalli*, 1995]

$$\sigma_1' - \sigma_3' = 2\sigma_v'(R' - 1)/(R' + 1), \tag{26}$$

where

$$R' = \sigma_1'/\sigma_3' = \left[\left(1 + \mu^2\right)^{1/2} - \mu\right]^{-2}. \tag{27}$$

For the case of a normal fault and a thrust fault, σ_v' equals σ_1' and σ_3', respectively. The minimum differential stress to activate sliding is

$$\sigma_1' - \sigma_3' = \sigma_v'(R' - 1)/R' \tag{28}$$

for a normal fault and

$$\sigma_1' - \sigma_3' = \sigma_v'(R' - 1) \tag{29}$$

for a thrust fault. Effective overburden pressure is given by

$$\sigma_v' = \rho_s g z(1 - \lambda), \tag{30}$$

where ρ_s is solid density, g is gravitational acceleration, z is depth, and λ is the pore fluid factor, i.e., the ratio of pore fluid pressure to overburden pressure, which for our case takes the value 0.36. The minimum shear stress required to activate frictional sliding is

$$\tau = {}^{1}\!/_{2}(\sigma_1' - \sigma_3')\sin\left[\tan^{-1}(1/\mu)\right], \tag{31}$$

where $(\sigma_1 - \sigma_3)$ is given by (26), (28), and (29) for strike slip faults, normal faults, and thrust faults, respectively.

[35] To describe crystal plastic flow at greater depth we use the creep equation for wet quartzite of *Luan and Paterson* [1992], rewritten for the case of simple shear as

$$\dot{\gamma} = 3^{(n+1)/2} A^* \tau^n \exp\left(\frac{-Q}{RT}\right), \tag{32}$$

where $n = 2.3$, $A = 1.8 \times 10^{-18}$, and the activation energy Q is 150 kJ mole^{-1}.

[36] For the frictional-viscous flow mechanism described above we assume a foliated quartz-mica mylonite. In accordance with typical mylonitic microstructures the angle α is taken to be 20°, the grain size d is taken to be 25 μm, and the grain aspect ratio is taken to be 4. As in the case of kaolinite, the appropriate value for the apparent grain boundary friction coefficient is not well constrained. Conventional friction experiments are again of little use, because these experiments typically measured the frictional strength of phyllosilicate gouge, whereas the local contact friction coefficient is required. From the tribology literature, it seems that the friction coefficient of a flat, ideally oriented mica grain may be as low as 0.01 in the presence of water [*Israelachvili*, 1992]. However, this value was measured at fairly low normal stress, and whether it is realistic for natural situations is not clear. An upper bound for the sliding strength of phyllosilicate foliae may be formed by the strength of micas undergoing basal glide. The strengths of mica single crystals oriented for glide are very low (<10 MPa) at geologic deformation rates [*Shea and Kronenberg*, 1992; *Wintsch et al.*, 1995]. Deformation studies of basal dislocation glide in muscovite single crystals at 400°C show that strength is pressure sensitive up to 50 MPa normal stress and can be approximated by an apparent friction coefficient of ~0.12 over pressures corresponding to the depth range 0–15 km [*Mares and Kronenberg*, 1993]. In this study, we take a value for the grain boundary friction coefficient of 0.2, but in actual fact it may be lower, and more detailed work is needed on this subject.

[37] For the solubility of quartz the relation reported by *Rimstidt* [1997] was used, neglecting small effects of pressure [*Fournier and Potter*, 1982]. The interface reaction rate constants k_{diss} and k_{prec} for quartz were taken from *Bird et al.* [1986]. Here the rate constant is referred to a standard system of 1 m^2 of surface area subjected to 1 kg of water. As pointed out by *Paterson* [1995], to express the values obtained by *Bird et al.* [1986] in m s^{-1}, the value for the dissolution coefficient must be divided by ρ_s, and the value of the precipitation coefficient must be multiplied by the product $M_s\ \Omega_s C^{-1}$.

[38] The diffusion coefficient of fluid-filled grain boundaries undergoing pressure solution is the subject of long-standing debate. Pressure solution compaction experiments indicate a grain boundary diffusion process similar to ionic diffusion in a static fluid, but the absolute value of the grain boundary diffusion coefficient may be 2 to 3 orders of magnitude lower than that of ionic diffusion in a bulk fluid [*Gratier and Guiget*, 1986; *Spiers et al.*, 1990]. On the other hand, grain boundary coefficients determined in novaculites by *Farver and Yund* [1991] at temperatures of 450–800°C yield much lower diffusion coefficients, and an activation energy of ~113 kJ mole^{-1} i.e., much higher than that for ionic diffusion. We have followed *Nakashima* [1995] in taking an activation energy characteristic of ionic diffusion (i.e., ~20 kJ mole^{-1}) and extrapolated the value for

diffusivity obtained by *Gratier and Guiget* [1986]. However, it should be stressed here that the grain boundary diffusivity is an ill-constrained parameter, and determination of grain boundary diffusivity during pressure solution in both synthetic and natural materials is an important future research goal.

[39] The relation between depth and fault normal stress is more complicated in the case of frictional-viscous behavior than in the frictional case, because the apparent coefficient of friction itself, and hence the contribution of the differential stress to the normal stress on the fault, is expected to be a function of depth. The normal stress on the fault is given by

$$\sigma_n' = \frac{1}{2}(\sigma_1' + \sigma_3') - \frac{1}{2}(\sigma_1' - \sigma_3')\cos\left[\tan^{-1}\left(1/\mu_{\text{app}}\right)\right]. \qquad (33)$$

For the case of a strike slip fault, using the relations

$$\sigma_v' = \frac{1}{2}(\sigma_1' + \sigma_3') \qquad (34)$$

and

$$\tau = \frac{1}{2}(\sigma_1' - \sigma_3')\sin\left[\tan^{-1}\left(1/\mu_{\text{app}}\right)\right] = \mu_{\text{app}}\sigma_n', \qquad (35)$$

σ_n' can be written in terms of the apparent friction coefficient μ_{app}, and the overburden pressure σ_v' can be written as

$$\sigma_n' = \left(1 + \mu_{\text{app}}^2\right)^{-1}\sigma_v'. \qquad (36)$$

Similarly, for a normal fault, using $\sigma_v' = \sigma_l'$ and (28), the relation between normal stress and overburden pressure is

$$\sigma_n' = \frac{1}{2}\sigma_v'\left[\left(1 + {}^{1}/_{R'}\right) - \left(1 - {}^{1}/_{R'}\right)\cos\left(\tan^{-1}\mu_{\text{app}}^{-1}\right)\right]. \qquad (37)$$

For a thrust fault, using $\sigma_v' = \sigma_3'$ the relation becomes

$$\sigma_n' = \frac{1}{2}\sigma_v'\left[(R' + 1) - (R' - 1)\cos\left(\tan^{-1}\mu_{\text{app}}^{-1}\right)\right]. \qquad (38)$$

Note that in this case, although an apparent friction coefficient is used, a strictly linear relation between τ and σ_n is not implied, since μ_{app} may vary with depth because of the increased contribution of pressure solution with increasing temperature. It follows from the above that the relation between σ_n' and σ_v' depends on the apparent friction coefficient. Hence the exact relation can only be obtained by iteration. However, in section 5.2 we will simply assume that the faults are optimally oriented for Byerlee's law friction at all crustal depths. This seems reasonable since the faults will generally form in intact material with a high coefficient of internal friction, whereas the "weak" behavior as modeled here only arises after sufficient strain has been accumulated to allow weakening [cf. also *Bos and Spiers*, 2001]. Hence the relation between overburden pressure and fault normal stress is given by (36), (37), and (38), assuming an apparent friction coefficient of 0.75.

5.2. Strength Profiles Incorporating Pressure Solution-Controlled Frictional-Viscous Behavior

[40] Before presenting our model predictions, it should be noted that the quality of the model predictions is, as always, determined by the quality of the model assumptions and input data. In this case, the uncertainties in many of the input parameters, in particular grain boundary friction and diffusion coefficients, are considerable, and there is a great need for systematic experimental work on this. Therefore the strength profiles presented here should be viewed with caution. With these reservations, we present crustal strength profiles for the four cases mentioned in section 5.1 in Figures 8a–8d. It should be noted that, in our view, like all strength profiles, Figures 8a–8d should be seen as representing the strength of fault rock material as a function of depth at the prescribed conditions. The relation between the strength of the fault zone material and the actual strength of the fault zone may not be straightforward because of the geometrical complexities of natural fault zones. Research on this complex issue is still in its infancy. Therefore strength profiles can give at best a semi-quantitative estimate of crustal strength, and Figure 8 should be seen primarily as illustrating quantitatively the effect of pressure solution-controlled flow in leading to weakening of fault zone material with respect to the "Byerlee's law plus quartzite plasticity" rheology commonly employed in numerical modeling studies.

[41] In Figure 8, "Byerlee's law" friction is shown using a dashed line, whereas dislocation creep curves for different strain rates (as indicated) are shown using shaded lines. The strength as predicted by our model is shown as solid lines for strain rates of 10^{-10} and 10^{-12} s^{-1}. This corresponds to a fault zone sliding at ~30 mm yr^{-1}, such as the San Andreas Fault, where sliding is accommodated in a fault zone of 10 and 1000 m wide, respectively. Curves are shown for diffusion-controlled pressure solution, since the model results indicate that diffusion is the rate-limiting step in pressure solution at all depths in our model. In natural fault zones, strain rate is not expected to be constant with depth; rather, shear zones are known to widen with increasing depth, leading to a decrease in average strain rate with depth [*Sibson*, 1977, 1983]. As a crude way of incorporating this in discussing our model results, we tentatively assume a strain rate of 10^{-12} s^{-1} in the lower crust where dislocation creep dominates, and a strain rate of 10^{-10} s^{-1} in phyllosilicate-rich shear zones in the middle-to-upper crust, so a crustal strength profile is outlined by the bold lines in Figure 8.

[42] The model shows a transition from behavior closely resembling Byerlee's law at shallow depths (corresponding to regime 3 in Figure 6) to behavior where strength is controlled by grain boundary friction (regime 1 in Figure 6) at greater depths. The transition region is the pressure solution-controlled regime (regime 2 in Figure 6), where mechanical behavior is strongly rate-sensitive as well as normal stress sensitive. For the conditions and strain rates considered above, this regime dominates over the depth range 5–20 km. Indeed, this is the depth range where solution transfer processes are expected to be active as inferred from microstructural observations [*Groshong*, 1975; *McClay*, 1977; *Rutter*, 1983; *Schwarz and Stöckhert*, 1996]. The depth at which frictional-viscous behavior is expected varies strongly with the geotherm and the type of fault. Nevertheless, in all cases the rate-sensitive behavior occurs at depths where temperatures are too low for dislocation creep to be active at significant rate. Thus our model predicts that a significant range of the crust should show mechanical behavior that is both strain rate and normal stress dependent. At depths greater than 15–20 km, the model predicts that dislocation creep takes over as the strength-determining mechanism. Because of the lower stresses supported by the frictional-viscous mechanism, the depth at which dislocation creep becomes the strength-determining mechanism is shifted to slightly deeper levels in our model compared with a classical two-mechanism strength profile.

[43] The least well-constrained parameters in the model are the grain boundary diffusion coefficient and the grain boundary friction coefficient. The model sensitivity to the grain boundary diffusion coefficient can be estimated directly from the strain rate sensitivity in Figure 8, since an order-of-magnitude increase in strain rate has the same effect as an order-of-magnitude decrease in grain boundary diffusion coefficient (see equation

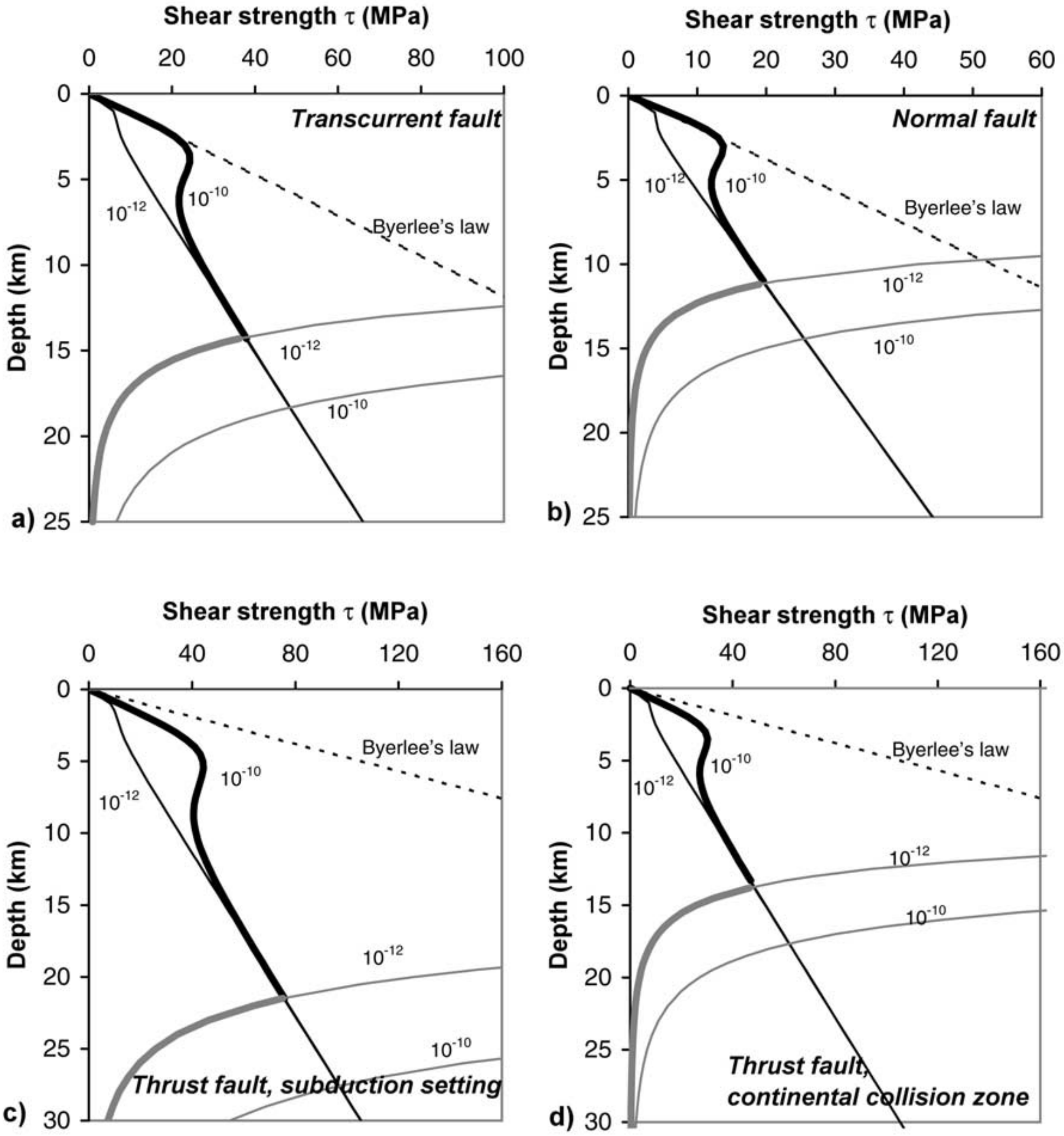

Figure 8. Model predictions of shear strength versus depth for phyllosilicate-bearing fault rock in different tectonic settings. Strength profiles are shown for (a) a transcrustal strike-slip fault zone, (b) a normal fault zone in an extensional region, (c) a thrust fault zone in a subduction setting, and (d) a thrust fault zone in a typical continental collision zone. Temperature gradients used are 25°, 35°, 15°, and 25°C km^{-1}, respectively. The dashed lines shows frictional "Byerlee's law" behavior, with a friction coefficient μ of 0.75. The shaded lines show flow laws for quartz dislocation creep for strain rates of 10^{-10} and 10^{-12} s^{-1}. The solid lines show predictions of our model, for the case of diffusion-controlled pressure solution, for strain rates of 10^{-10} and 10^{-12} s^{-1}. Crudely taking into account the widening of shear zones with depth, a typical strength profile for fault rock in high-strain fault zones would be given by the weakest of the Byerlee's law line, the pressure solution creep line for a strain rate of 10^{-10} s^{-1}, and the dislocation creep line for 10^{-12} s^{-1} at any given depth. Note that our model predicts pressure solution-controlled creep to dominate rheology in high-strain fault zones at depths ranging from 5–20 km.

(17)). The value of the diffusion coefficient has a strong effect on the depth of the transition region between Byerlee's law behavior and behavior controlled by grain boundary friction. The grain boundary friction coefficient determines the slope of the strength versus depth line below the transition region and hence has a strong influence on the total integrated strength of the crust. The depth of the transition, however, is not very sensitive to the grain boundary friction coefficient.

[44] The model shows that the presence of foliated, fine-grained phyllosilicate-bearing shear zones, undergoing deformation by pressure solution-accommodated sliding, leads to significant modification of the strength envelope, in particular in the region where classical two-mechanism strength profiles (as defined by the Byerlee's law line and the dislocation creep curves in Figure 8) predict a pronounced strength maximum. In the strength profile no pronounced peak is predicted by our model, and the increase of

strength with depth is much more gradual than in two-mechanism strength profiles. In addition, significant weakening with respect to classical two-mechanism strength profiles is predicted in all tectonic regimes. The effect is strongest in a high pressure-low temperature (HP-LT) "subduction" setting (Figure 8c) because of the low-temperature dependence of pressure solution relative to dislocation creep. Here our model predicts weakening by more than a factor 4 around the brittle-ductile transition, but significant weakening, by a factor of 2–3, is also predicted in the other scenarios. For finer-grained fault rocks, or a lower value of the grain boundary friction coefficient, the weakening effect would be even larger. Deformation of quartz phyllonites at stress levels below those needed to activate dislocation creep has been inferred from field observations, in particular in HP-LT environments [*Schwarz and Stöckhert*, 1996; *Imber et al.*, 1997; *Stöckhert et al.*, 1999; *Stewart et al.*, 2000]. Both the inferred depth range and the inferred shear stress level are broadly consistent with our model predictions.

[45] The importance of pressure solution-controlled flow of fine-grained fault rock in allowing weakening with respect to Byerlee's law friction has been stressed for two decades [*Sibson*, 1977; *Rutter and Mainprice*, 1979; *Sibson*, 1983; *Chester and Higgs*, 1992; *Hickman et al.*, 1995]. The model developed here allows for the first time quantitative incorporation of this mechanism into geodynamic models for crustal tectonics. In geodynamic modeling studies, rheology is usually expressed in the simplest possible way, to avoid excessive numerical cost. While it would be preferable to incorporate the rheological laws developed here directly into numerical models of crustal tectonics, a low-cost alternative would be to tentatively assume an apparent friction coefficient for highly strained crust of ~0.25–0.35. This value could then apply to the crust up to depths where dislocation creep becomes active. A way to incorporate the evolution of mechanical behavior with increasing strain would then be to allow the apparent friction coefficient to evolve from ~0.75 for unstrained rock to ~0.3 for highly strained material. This is likely to significantly influence tectonic modeling results, probably favoring strong localization of deformation into strain-weakening shear zones, as observed in natural tectonic belts.

[46] The weakening with respect to Byerlee's law for high-strain fault zones predicted by our model may aid in explaining the low heat flow in the San Andreas Fault area. Here, the lack of a measurable heat flow anomaly in the vicinity of the fault is inferred to imply an average frictional traction on the fault of 20 MPa or lower [*Lachenbruch and Sass*, 1992], i.e., far lower than the 90-260 MPa predicted from Byerlee's law. For the strike-slip case (Figure 8a) our model indeed predicts an average crustal strength of a few tens of megapascals over the depth range 0–20 km, based on an assumed 10-m-wide shear zone at these depths. Note, however, that this value strongly depends on the assumed value for the grain boundary friction coefficient, which is a poorly constrained parameter.

6. Conclusions

1. A microphysical model for deformation of foliated, phyllosilicate-rich fault rock by a mechanism of sliding along phyllosilicate foliae accommodated by pressure solution predicts three regimes of rheological behavior: a regime of frictional behavior at high shear strain rates, a regime of frictional-viscous behavior at intermediate shear strain rates, and, again, a regime of frictional behavior at low sliding velocities. Fault strength is predicted to be normal stress dependent at all shear strain rates.

2. The model describes our previously reported experimental data on the halite + kaolinite system reasonably well, particularly at low (<50%) clay contents and sliding velocities of 1 μm s^{-1} and lower. This supports earlier inferences that these materials deformed by pressure solution-accommodated sliding along kaolinite foliae.

3. When applied to the crust, the model predicts that the strength of foliated, phyllosilicate-bearing fault rock is dominated by pressure solution-controlled frictional-viscous behavior at depths ranging from 5–20 km, depending on tectonic setting. This is broadly consistent with inferences from field observations on natural, phyllosilicate-rich fault zones.

4. The model predicts that the development of foliated, phyllosilicate-bearing shear zones may lead to significant rheological weakening, by up to a factor 4.5 with respect to conventional crustal strength envelopes. Since crustal strength is thought to be strongly controlled by the presence of large shear zones, our results question the applicability of conventional strength profiles for modeling crustal tectonic processes.

5. The crustal strength profiles predicted by our model suggest that in numerical models for geodynamic processes the strength of fault rock of highly deformed regions should be approximated using our equation for frictional-viscous behavior instead of using conventional strength profiles, since the latter may significantly overestimate fault rock strength. Alternatively, and numerically more cost effective, usage of an apparent friction coefficient of 0.25–0.35 for the frictional part of the strength envelope is suggested.

6. The quantitative predictions of our model rely heavily on grain contact scale parameters such as grain boundary diffusion and friction coefficients. However, the underlying processes are poorly understood, and the corresponding coefficients are not well constrained. Future work should be aimed at obtaining more reliable data on grain contact parameters.

[47] **Acknowledgments.** Hans de Bresser and Colin Peach are thanked for discussions. We also thank Mervyn Paterson and Rick Sibson for their reviews, which considerably improved the paper.

References

Bird, G., J. Boon, and T. Stone, Silica transport during steam injection into oil sands, 1, Dissolution and precipitation kinetics of quartz: New results and review of existing data, *Chem. Geol.*, *54*, 69–80, 1986.

Bos, B., and C. J. Spiers, Pressure solution, phyllosilicates, and the strength of mature faults, *EOS Trans. AGU*, *80*(46), F1055, 1999.

Bos, B., and C. J. Spiers, Effect of phyllosilicates on fluid-assisted healing of gouge-bearing faults, *Earth Planet. Sci. Lett.*, *184*, 199–210, 2000.

Bos, B., and C. J. Spiers, Experimental investigation into the microstructural and mechanical evolution of phyllosilicate-bearing fault rock under conditions favouring pressure solution, *J. Struct. Geol.*, *23*, 1187–1202, 2001.

Bos, B., C. J. Peach, and C. J. Spiers, Frictional-viscous flow of simulated fault gouge caused by the combined effects of phyllosilicates and pressure solution, *Tectonophysics*, *327*, 173–193, 2000.

Byerlee, J., Friction of rocks, *Pure Appl. Geophys.*, *116*, 615–627, 1978.

Chester, F. M., A rheologic model for wet crust applied to strike-slip faults, *J. Geophys. Res.*, *100*, 13,033–13,044, 1995.

Chester, F. M., and N. G. Higgs, Multimechanism friction constitutive model for ultrafine quartz gouge at hypocentral conditions, *J. Geophys. Res.*, *97*, 1859–1870, 1992.

De Groot, S. R., and P. Mazur, *Non-Equilibrium Thermodynamics*, 510 pp., North-Holland, New York, 1962.

De Meer, S., and C. J. Spiers, Uniaxial compaction creep of wet gypsum aggregates, *J. Geophys. Res.*, *102*, 875–891, 1997.

Farver, J. R., and R. A. Yund, Measurement of oxygen grain boundary diffusion in natural, fine grained, quartz aggregates, *Geochim. Cosmochim. Acta*, *55*, 1597–1607, 1991.

Fournier, R. O., and R. W. Potter, An equation correlating the solubility of quartz in water from 25° to 900°C at pressure up to 10,000 bars, *Geochim. Cosmochim. Acta*, *46*, 1969–1973, 1982.

Goetze, C., and B. Evans, Stress and temperature in the bending lithosphere as constrained by experimental rock mechanics, *Geophys. J. R. Astron. Soc.*, *59*, 463–478, 1979.

Govers, R., and M. J. R. Wortel, Extension of stable continental lithosphere and the initiation of lithosphere scale faults, *Tectonics*, *14*, 1041–1055, 1995.

Gratier, J. P., and R. Guiget, Experimental pressure solution-deposition on quartz grains: The crucial effect of the nature of the fluid, *J. Struct. Geol.*, *8*, 845–856, 1986.

Groshong, R. H., Fractures and pressure solution in natural single-layer folds, *Geol. Soc. Am. Bull.*, *86*, 1363–1376, 1975.

Handy, M. R., The solid state flow of polymineralic rock, *J. Geophys. Res.*, *95*, 8647–8661, 1990.

Handy, M. R., S. B. Wissing, and L. E. Streit, Frictional-viscous flow in mylonite with varied bimineralic composition and its effect on lithospheric strength, *Tectonophysics*, *303*, 175–191, 1999.

Hickman, S., R. Sibson, and R. Bruhn, Introduction to special section: Mechanical involvement of fluids in faulting, *J. Geophys. Res.*, *100*, 12,831–12,840, 1995.

Hickman, S. H., and B. Evans, Kinetics of pressure solution at halite-silica interfaces and intergranular clay films, *J. Geophys. Res.*, *100*, 13,113–13,132, 1995.

Imber, J., R. E. Holdsworth, C. A. Butler, and G. Lloyd, Fault-zone weakening processes along the reactivated Outer Hebrides Fault Zone, Scotland, *J. Geol. Soc. London*, *154*, 105–109, 1997.

Israelachvili, J. N., Adhesion forces between surfaces in liquids and condensable vapours, *Surf. Sci. Rep.*, *14*, 109–159, 1992.

Kawamoto, E., and T. Shimamoto, The strength profile for bimineralic shear zones: An insight from high-temperature shearing experiments on calcite-halite mixtures, *Tectonophysics*, *295*, 1–14, 1998.

Kohlstedt, D. L., B. Evans, and S. J. Mackwell, Strength of the lithosphere: Constraints imposed by laboratory experiments, *J. Geophys. Res.*, *100*, 17,587–17,602, 1995.

Kronenberg, A. K., S. H. Kirby, and J. Pinkston, Basal slip and mechanical anisotropy of biotite, *J. Geophys. Res.*, *95*, 19,257–19,278, 1990.

Lachenbruch, A. H., and J. H. Sass, Heat flow and energetics of the San Andreas fault zone, *J. Geophys. Res.*, *85*, 6185–6223, 1980.

Lachenbruch, A. H., and J. H. Sass, Heat flow from Cajon Pass, fault strength, and tectonic implications, *J. Geophys. Res.*, *97*, 4995–5015, 1992.

Lehner, F. K., Thermodynamics of rock deformation by pressure solution, in *Deformation Processes in Minerals, Ceramics and Rocks*, edited by D. J. Barber, and P. D. Meredith, pp. 296–333, Unwin Hyman, Boston, Mass., 1990.

Lehner, F. K., and J. Bataille, Nonequilibrium thermodynamics of pressure solution, *Pure Appl. Geophys.*, *122*, 53–85, 1984/1985.

Lister, G. S., and A. W. Snoke, S-C Mylonites, *J. Struct. Geol.*, *6*, 617–638, 1984.

Luan, F. C., and M. S. Paterson, Preparation and deformation of synthetic aggregates of quartz, *J. Geophys. Res.*, *97*, 301–320, 1992.

Mares, V. M., and A. K. Kronenberg, Experimental deformation of muscovite, *J. Struct. Geol.*, *15*, 1061–1075, 1993.

McClay, K. R., Pressure solution and Coble creep in rocks and minerals: A review, *J. Geol. Soc. London*, *134*, 57–70, 1977.

Morrow, C. A., D. E. Moore, and D. A. Lockner, The effect of mineral bond strength and adsorbed water on fault gouge frictional strength, *Geophys. Res. Lett.*, *27*, 815–818, 2000.

Nakashima, S., Diffusivity of ions in pore water as a quantitative basis for rock deformation rate estimates, *Tectonophysics*, *245*, 185–203, 1995.

Paterson, M. S., A theory for granular flow accommodated by material transfer via an intergranular fluid, *Tectonophysics*, *245*, 135–151, 1995.

Prigogine, I., *Thermodynamics of Irreversible Processes*, John Wiley, New York, 1967.

Raj, R., Creep in polycrystalline aggregates by matter transport through a liquid phase, *J. Geophys. Res.*, *87*, 4731–4739, 1982.

Raj, R., and M. F. Ashby, On grain boundary sliding and diffusional creep, *Metall. Trans.*, *2*, 1113–1126, 1971.

Raj, R., and C. K. Chyung, Solution-precipitation creep in glass ceramics, *Acta Metall.*, *29*, 159–166, 1981.

Ranalli, G., *Rheology of the Earth*, 413 pp., Chapman and Hall, New York, 1995.

Ranalli, G., Rheology of the lithosphere in space and time, in *Orogeny Through Time*, edited by J.-P. Burg and M. Ford, pp. 19–38, *Geol. Soc. Spec. Publ.*, *54*, 1997.

Reinen, L. A., J. D. Weeks, and T. E. Tullis, The frictional behavior of lizardite and antigorite serpentinites: Experiments, constitutive models, and implications for natural faults, *Pure Appl. Geophys.*, *143*, 318–358, 1994.

Renard, F., and P. Ortoleva, Water films at grain-grain contacts: Debye-Hueckel, osmotic model of stress, salinity, and mineralogy dependence, *Geochim. Cosmochim. Acta*, *61*, 1963–1970, 1997.

Rimstidt, J. D., Quartz solubility at low temperatures, *Geochim. Cosmochim. Acta*, *61*, 2553–2558, 1997.

Rutter, E. H., The kinetics of rock deformation by pressure solution, *Phil. Trans. R. Soc. London, Ser. A.*, *283*, 203–219, 1976.

Rutter, E. H., The mechanical properties of kaolinite fault "gouge" at moderate confining pressure, 20°C, *Int. J. Rock Mech. Min. Sci. Geomech. Abstr.*, *16*, 407–410, 1979.

Rutter, E. H., Pressure solution in nature, theory and experiment, *J. Geol. Soc. London*, *140*, 725–740, 1983.

Rutter, E. H., and R. H. Maddock, On the mechanical properties of synthetic kaolinite/quartz fault gouge, *Terra Nova*, *4*, 489–500, 1992.

Rutter, E. H., R. H. Maddock, S. H. Hall, and S. H. White, Comparative microstructures of natural and experimentally produced clay-bearing fault gouges, *Pure Appl. Geophys.*, *124*, 3–30, 1986.

Rutter, E. H., and D. H. Mainprice, On the possibility of slow fault slip controlled by a diffusive mass transfer process, *Gerlands Beitr. Geophysik*, *88*, 154–162, 1979.

Schwarz, S., and B. Stöckhert, Pressure solution in siliciclastic HP-LT metamorphic rocks: Constraints on the state of stress in deep levels of accretionary complexes, *Tectonophysics*, *255*, 203–209, 1996.

Shea, W. T., and A. K. Kronenberg, Rheology and deformation mechanisms of an isotropic mica schist, *J. Geophys. Res.*, *97*, 15,201–15,237, 1992.

Shea, W. T., and A. K. Kronenberg, Strength and anisotropy of foliated rocks with varied mica contents, *J. Struct. Geol.*, *15*, 1097–1121, 1993.

Shimamoto, T., The origin of S-C mylonites and a new fault-zone model, *J. Struct. Geol.*, *11*, 51–64, 1989.

Sibson, R. H., Frictional constraints on thrust, wrench and normal faults, *Nature Phys. Sci.*, *249*, 542–543, 1974.

Sibson, R. H., Fault rocks and fault mechanisms, *J. Geol. Soc. London*, *133*, 191–213, 1977.

Sibson, R. H., Continental fault structure and the shallow earthquake source, *J. Geol. Soc. London*, *140*, 741–767, 1983.

Spear, F. S., *Metamorphic Phase Equilibria and Pressure-Temperature-Time Paths*, 799 pp., Mineral. Soc. of Am., Washington, D. C., 1993.

Spiers, C. J., and R. H. Brzesowsky, Densification behaviour of wet granular salt: Theory versus experiment, in *Seventh Symposium on Salt*, pp. 83–92, Elsevier Sci., New York, 1993.

Spiers, C. J., and P. M. T. M. Schutjens, Densification of crystalline aggregates by fluid phase diffusional creep, in *Deformation Processes in Minerals, Ceramics and Rocks*, edited by D. J. Barber, and P. G. Meredith, pp. 334–353, Unwin Hyman, Boston, Mass., 1990.

Spiers, C. J., P. M. T. M. Schutjens, R. H. Brzesowsky, C. J. Peach, J. L. Liezenberg, and H. J. Zwart, Experimental determination of constitutive parameters governing creep of rocksalt by pressure solution, in *Deformation Mechanisms, Rheology and Tectonics*, edited by R. J. Knipe, and E. H. Rutter, *Geol. Soc. Spec Publ.*, *54*, 215–227, 1990.

Stewart, M., R. E. Holdsworth, and R. A. Strachan, Deformation processes and weakening mechanisms within the frictional-viscous transition zone of major crustal-scale faults: Insights from the Great Glen Fault Zone, Scotland, *J. Struct. Geol.*, *22*, 543–560, 2000.

Stöckhert, B., M. Wachmann, M. Küster, and S. Bimmerman, Low effective viscosity during high pressure metamorphism due to dissolution precipitation creep: the record of HP-LT metamorphic carbonates and siliciclastic rocks from Crete, *Tectonophysics*, *303*, 299–319, 1999.

White, S. H., S. E. Burrows, J. Carreras, N. D. Shaw, and F. J. Humphreys, On mylonites in ductile shear zones, *J. Struct. Geol.*, *2*, 175–187, 1980.

Wintsch, R. P., R. Christoffersen, and A. K. Kronenberg, Fluid-rock reaction weakening of fault zones, *J. Geophys. Res.*, *100*, 13,021–13,032, 1995.

Wood, D. M., *Soil Behaviour and Critical State Soil Mechanics*, 462 pp., Cambridge Univ. Press, New York, 1990.

B. Bos, TNO TPD Materials Technology, P.O. Box 595, 5600 AN Eindhoven, Netherlands. (bbos@tpd.tno.nl)

C. J. Spiers, High Pressure and Temperature Laboratory, Faculty of Earth Sciences, Utrecht University, P.O. Box 80 021, 3508 TA Utrecht, Netherlands.